JOURNAL OF MATERIAL SCIENCE **28** (1993) 5099–5111

A critical evaluation of theories for predicting microcracking in composite laminates

JOHN A. NAIRN, SHOUFENG HU, and JONG SEOK BARK
Material Science and Engineering, University of Utah, Salt Lake City, Utah 84112, USA

We present experimental results on 21 different layups of Hercules AS4 carbon fiber/3501-6 epoxy laminates. All laminates had 90° plies; some had them in the middle ($[(S)/90_n]_s$) while some had them on a free surface ($[90_n/(S)]_s$). The supporting sublaminates, (S), where $[0_n]$, $[\pm 15]$, or $[\pm 30]$. During tensile loading, the first form of damage in all laminates was microcracking of the 90° plies. For each laminate we recorded both the crack density and the complete distribution of crack spacings as a function of the applied load. By rearranging various microcracking theories we developed a master-curve approach that permitted plotting the results from all laminates on a single plot. By comparing master curve plots for different theories it was possible to critically evaluate the quality of those theories. We found that a critical-energy-release-rate criterion calculated using a two-dimensional variational stress analysis gave the best results. All microcracking theories based on a strength-failure criterion gave poor results. All microcracking theories using one-dimensional stress analyses, regardless of the failure criterion, also gave poor results.,

1. Introduction

When the 90° plies are relatively less stiff than the supporting plies, the first form of failure in $[(S)/90_n]_s$ or $[90_n/(S)]_s$ laminates (where (S) denotes any orthotropic sublaminate) is usually microcracking or transverse cracking of the 90° ply groups [1–24]. When the 90° plies are in the middle ($[(S)/90_n]_s$ laminates), those plies crack into an array of roughly periodic microcracks. When the 90° plies are on the outside ($[90_n/(S)]_s$ laminates), each 90° ply group cracks into an array of roughly periodic microcracks, but the two arrays are shifted from each other by half the average crack spacing [11, 25]. Typical damage states for $[(S)/90_n]_s$ and $[90_n/(S)]_s$ laminates are shown in Fig. 1.

The are many reasons for studying microcracking. Microcracks not only change the thermal and mechanical properties of the laminate [11, 26, 27], but they also present pathways through which corrosive agents may penetrate into the interior of the laminate [6]. Perhaps most importantly, microcracks act as nuclei for further damage such as delamination [1, 10, 14, 28], longitudinal splitting [5, 6], and curved microcracks [21, 29]. Because microcracks are the precursors to the cascade of events that leads to laminate failure, we have little hope of understanding laminate failure or of predicting long-term durability if we do not first develop a thorough understanding of the phenomenon of microcracking. To understand microcracking we must be able to predict the initiation of microcracking, the increase in microcrack density with increasing load, the conditions under which microcracks nucleate other forms of damage, the differences between $[(S)/90_n]_s$ and $[90_n/(S)]_s$ laminates, and the effect of residual thermal stresses [30]. A successful microcracking analysis should be fundamental and not resort to empiricism. A typical empirical analysis introduces *in situ* parameters such as layup dependent ply strengths. The use of such parameters destroys the useful predictive capabilities of an analysis.

Because of the importance of understanding microcracking, there has been much work in the post 15 years aimed at predicting experimental observations. The first step towards understanding microcracking is to consider the effect of microcracks on the stresses and strains in the laminate. Most stress analyses are one-dimensional [1, 2, 5, 12, 31–39]. For reasons given below, we refer to analysis that ignores the through-the-thickness stresses as a one-dimensional analysis. Hashin used variational mechanics to develop the first two-dimensional analysis of the stresses in microcracked $[0_m/90_n]_s$ laminates [40, 41]. Nairn *et. al.* extended Hashin's results to include residual thermal stresses [23, 42], to handle the more general $[(S)/90_n]_s$ laminates [28], and to analyze laminates with surface 90° plies ($[90_n/(S)]_s$ laminates) [25]. The second step towards understanding microcracking is to propose a failure criterion and use some calculated stress state to predict experimental results. Some workers have proposed strength models which claim that a microcrack forms when the longitudinal stress in the 90° plies reaches the transverse strength of those plies [1, 4, 12, 13, 22, 34, 43]. More recent work has proposed energy models which claim that a microcrack forms when the energy release rate reaches a critical value [3, 5, 17, 20, 23, 25, 30, 35–37, 39, 42].

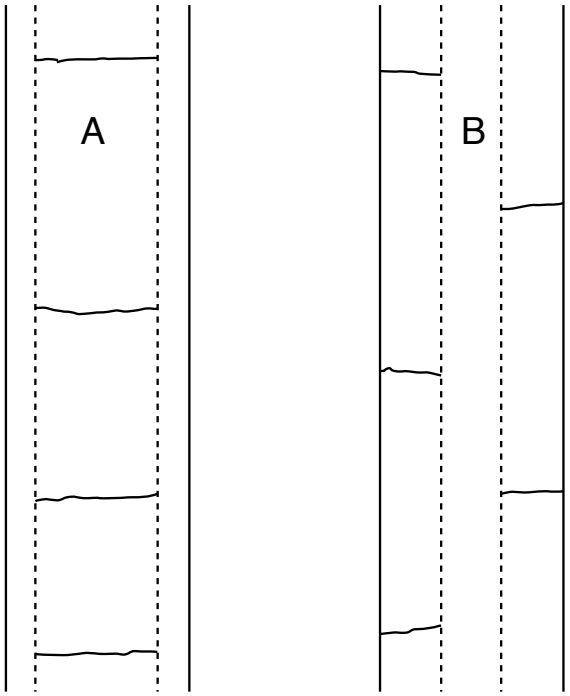

Fig. 1. Sketches of actual damage in cross-ply laminates. A. Roughly periodic array of microcracks in a $[0/90_4]_s$ laminate. B. Antisymmetric or staggered microcracks in a $[90_4/0_2]_s$ laminate.

There are numerous opinions regarding the most appropriate method for analyzing microcracking experiments. To provide a critical test of microcracking theories, we measured the crack density as a function of applied load for 21 different layups of Hercules AS4 carbon fiber/3501-6 epoxy composites. The range of laminates included $[(S)/90_n]_s$ and $[90_n/(S)]_s$ laminates. The supporting sublaminates (S) included $[0_n]$, $[\pm 15]$ and $[\pm 30]$ sublaminates. A *fundamental* microcracking analysis should be able to take a single material property, such as transverse ply strength or transverse ply fracture toughness, and predict the results from all 21 laminates. To facilitate comparison of various microcracking theories, we developed a master-curve method. In brief, the various stress analyses were used to develop scaling laws that permit plotting the results from all laminates on a single linear master plot. The accuracy with which any analysis conforms to the linear master plot predictions quickly reveals the adequacy on that analysis. Our findings were that the only satisfactory analysis is one that uses two-dimensional variational mechanics stress analysis and an energy release rate failure criterion. All theories that rely on one-dimensional stress analyses gave particularly poor results.

2. Materials and methods

Static tensile tests were run on Hercules AS4 carbon fiber/3501-6 epoxy matrix composites. The material was purchased from Hercules in prepreg form and autoclaved cured at 177°C according to manufacturer's recommendations. We made eight cross-ply layups with 90° plies in the middle—$[0/90]_s$, $[0/90_2]_s$, $[0/90_4]_s$, $[0_2/90]_s$, $[0_2/90_2]_s$, $[0_2/90_4]_s$, $[\pm 15/90_2]_s$, and $[\pm 30/90_2]_s$. We made 13 cross-ply layups with surface 90° plies—$[90/0/90]_T$, $[90/0]_s$, $[90/0_2]_s$, $[90/0_4]_s$, $[90_2/0/90_2]_T$, $[90_2/0]_s$, $[90_2/0_2]_s$, $[90_2/0_4]_s$, $[90_2/\pm 15]_s]$, $[90_2/\pm 30]_s]$, $[90_3/0]_s$, $[90_3/0_2]_s$, and $[90_4/0_2]_s$. Specimens nominally 12 mm wide and 150 mm long with thicknesses determined by the stacking sequences (about 0.125 mm per ply) were cut from the cured laminates. All specimens had 19 mm by 12 mm aluminum end tabs epoxied in place with Hysol 9230 epoxy.

All tensile tests were run in displacement control, at a rate of 0.005 mm/sec, on a Minnesota Testing Systems (MTS) 25 kN servohydraulic testing frame. Load *vs.* displacement data was collected on an IBM PC-XT that was interfaced to and MTS 464 Data Display Device. While testing each specimen, the experiment was periodically stopped and examined by optical microscopy. For $[(S)/90_n]_s$ laminates we mapped the

complete distribution of microcrack spacings on either edge of the specimen. To get an average crack density, we averaged the densities on the two specimen edges. For $[90_n/(S)]_s$ laminates, microcracks could be seen on the edges and on the specimen faces. We mapped the complete distribution of microcrack spacings in each of the two surface 90° ply groups. To get an average crack density, we averaged the densities of the two 90° ply groups. The specimens were continually reloaded into the MTS frame and loaded to higher displacements until the end tabs failed, the specimen failed, or delamination began.

3. Experimental observations

To provide a critical test of microcracking theories we tested 21 different layups of AS4/3501-6 laminates. Eight of the tested laminates had 90° plies in the middle. Many previous investigators have reported results for such $[(S)/90_n]_s$ laminates. The results for our tests agreed with previous experimental observations except that we have the largest number of layups for a single material ever included in a single study. The $[(S)/90_n]_s$ laminates all failed first by a roughly periodic array of microcracks in the 90° plies (see Fig. 1A). The microcracks stopped at the $(S)/90$ interface with little tendency to cause delamination until the crack density and applied strain became sufficiently high. The first microcracks occurred at lower strain for laminates with thicker 90° ply groups In contrast, the maximum crack density observed at high strains was larger for laminates with thinner 90° ply groups. The microcrack density as a function of applied load for these laminates is discussed in Section 4. The reader is referred to [23] for typical raw plots of crack density *vs.* applied load in $[(S)/90_n]_s$ laminates.

The microcracking properties of $[90_n/(S)]_s$ laminates are much less commonly studied (see [5, 8, 11, 22]) Thirteen of our tested laminates had 90° plies on the free surfaces — the $[90_n/(S)]_s$ laminates. They all developed a roughly periodic array of microcracks in each of the surface 90° ply groups. As shown in Fig. 1B, the microcracks in one 90° ply group where systematically staggered from the microcracks in the other 90° ply group. Some typical raw plots of crack density *vs.* applied load in $[90_n/(S)]_s$ laminates are in Fig. 2. As in $[(S)/90_n]_s$ laminates, the first microcracks occurred at lower strains for laminates with thicker 90° ply groups. The absolute value of the microcracking initiation strain, however, was lower for $[90_n/(S)]_s$ laminates than it was for the companion $[(S)/90_n]_s$ laminate. This general tend was sometimes obscured by scatter at low crack densities that could by attributed to laminate flaws [23]. At high crack densities, the damage state in $[90_n/(S)]_s$ laminates showed a lower crack density than the damage state in the companion $[(S)/90_n]_s$ laminates. The differences were significant—typically a factor of two. Although early microcracks stopped at the $(S)/90$ interface, $[90_n/(S)]_s$ laminates should a greater tendency to delaminate than $[(S)/90_n]_s$ laminates. The tendency towards delamination increased as the thickness of the 90° plies increased. This qualitative prediction agrees with stress analysis predictions in [25]. In the three laminates with the thickest 90° ply groups, $[90_3/0]_s$, $[90_3/0_2]_s$, and $[90_4/0_2]_s$, delamination started soon after the first microcrack. Because we could not obtain sufficient microcrack density data for these laminates, they were ignored in microcracking analysis described in Section 4..

4. Analysis results

4.1. $[(S)/90_n]_s$ laminates: Energy release rate analysis

We first consider $[(S)/90_n]_s$ laminates under an axial stress, σ_0, in the x direction. Under most experimental conditions, the microcracks that form in the 90° plies span the entire cross-section of those plies as through-the-width cracks [30]. In the presence of only through-the-width damage, the stress analysis is approximately two-dimensional in the (x–z) plane or the laminate edge plane. The coordinate system of the stress analysis is shown in Fig. 3A. Hashin used variational mechanics to derive the first two-dimensional, analytical stress analysis for the (x–z) plane of a microcracked $[0_m/90_n]_s$ laminate [40, 41]. His only assumption is that the x-axis normal stresses in the 0° and the 90° plies are functions of x, but independent of z. He determines the best approximate stress state, under his one assumption, by minimizing the total complementary energy. Nairn and co-workers extended Hashin's analysis to include residual thermal stresses and to handle general $[(S)/90_n]_s$ laminates [23, 28, 42].

The variational mechanics analysis determines all components of the stress tensor in the (x–z) plane. In this paper, we only require the tensile stress in the 90° plies. The result from [23] is

$$\sigma_{xx}^{(1)}(\xi) = \sigma_{x0}^{(1)}\left(1 - \phi(\xi)\right) \tag{1}$$

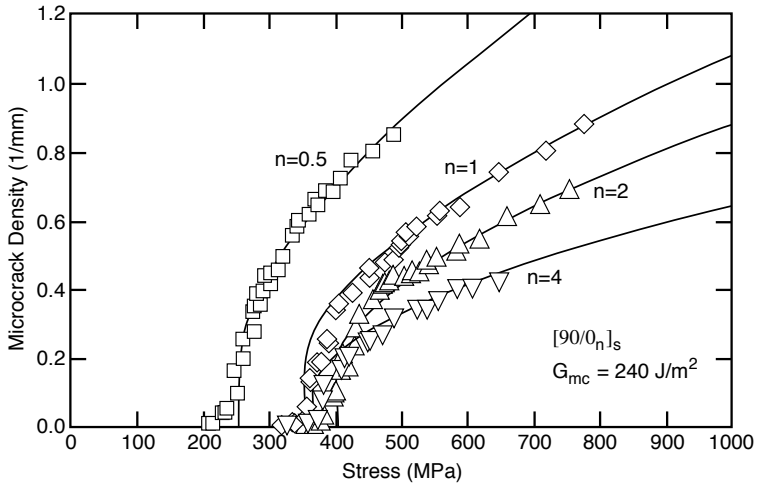

Fig. 2. Microcrack density as a function of applied load in a series of AS4/Hercules 3501-6 carbon/epoxy laminates. The symbols are experimental data points. The smooth lines are predictions using the variational mechanics energy release rate theory and $G_{mc} = 240$ J/m^2

where subscript (1) denotes the 90° plies, $\sigma_{x0}^{(1)}$ is the tensile stress in the 90° plies in the absence of microcracking damage, and $\phi(\xi)$ is a function determined by the variational mechanics analysis (see the Appendix). Equation 1 and all subsequent equations are written in terms of a dimensionless x-direction coordinate defined as

$$\xi = \frac{x}{t_1} \tag{2}$$

where t_1 is the semi-thickness of the 90° ply group. For a linear thermoelastic material we can write

$$\sigma_{x0}^{(1)} = k_m^{(1)}\sigma_0 + k_{th}^{(1)}T \tag{3}$$

where σ_0 is the total applied axial stress and $T = T_s - T_0$ is the difference between the specimen temperature, T_s and the effective stress-free temperature, T_0. (Note that Refs. [23, 25, 28, 40, 41, 42] define $\sigma_{x0}^{(1)} = k_m^{(1)}\sigma_0$ or as the mechanical load in 90° plies of the undamaged laminate. As expressed in Equation 3, we altered the definition of $\sigma_{x0}^{(1)}$ to also include the initial thermal stresses.) The terms $k_m^{(1)}$ and $k_{th}^{(1)}$ are the effective thermal and mechanical stiffnesses of the 90° plies. By a simple one-dimensional, constant-strain analysis they are

$$k_m^{(1)} = \frac{E_x^{(1)}}{E_c^0} \qquad \text{and} \qquad k_{th}^{(1)} = -\frac{\Delta\alpha}{C_1} \tag{4}$$

Here E_c^0 is the x-direction modulus of the laminate, $E_x^{(1)}$ is the x-direction modulus of the 90° plies, $\Delta\alpha = \alpha_x^{(1)} - \alpha_x^{(2)}$ is the difference between the x-direction thermal expansion coefficients of the 90° plies and the (S) sublaminate, and C_1 is a constant defined in the Appendix. Alternatively, $k_m^{(1)}$ and $k_{th}^{(1)}$ could be found by a laminated plate theory analysis of the undamaged analysis. The results, however, would only differ from Equation 4 by 2 to 5% [30].

To predict microcracking results, Liu and Nairn [23, 42] advocated an energy release rate failure criterion. In brief, the next microcrack is assumed to form when the total energy release rate associated with the formation of that microcrack, G_m, equals or exceed the microcracking fracture toughness of the material, G_{mc}. From the thermoelastic, variational mechanics stress state, the total energy release rate from [23] and [42] is

$$G_m = {\sigma_{x0}^{(1)}}^2 C_3 t_1 Y(D) \tag{5}$$

where C_3 is a constant defined in the Appendix and

$$Y(D) = LW\frac{d}{dA}\frac{\sum_{i=1}^N \chi(\rho_i)}{\sum_{i=1}^N \rho_i} = \frac{d}{dD}\Big(D\langle\chi(\rho)\rangle\Big) \tag{6}$$

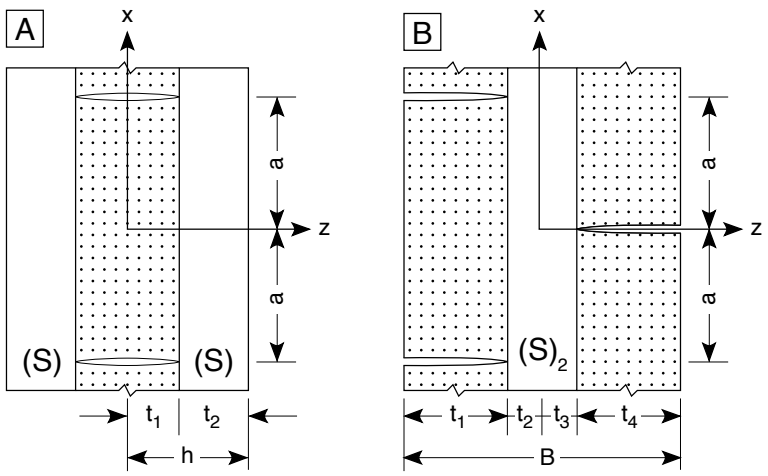

Fig. 3. Edge views of microcracks in the 90° plies of laminates. A: Two microcracks in a $[(S)/90_n]_s$ laminate. B: Three staggered microcracks in a $[90_n/(S)]_s$ laminate.

In Equation 6, $\chi(\rho)$ is a function determined by the variational analysis (see the Appendix), and the summation refers to a sample with N microcrack intervals having aspect ratios (a_i/t_1) or $\rho_1, \rho_2, \ldots, \rho_N$. $A = 2t_1LW$ is total microcrack surface area and $D = (2\langle\rho\rangle t_1)^{-1}$ is the average crack density, L is the sample length, and W is the sample width. The angular bracket notation implies an average of that quantity over the N microcrack intervals.

To use Equation 5, $Y(D)$ must be evaluated. Following Laws and Dvorak [37], Liu and Nairn [23, 42] evaluated $Y(D)$ for the discrete process of forming a new microcrack at dimensionless position $\xi = 2\delta - \rho_k$ in the k^{th} microcrack interval. The result is

$$Y(D) = \frac{\Delta D\langle\chi(\rho)\rangle}{\Delta D} = \chi(\rho_k - \delta) + \chi(\delta) - \chi(\rho_k) \tag{7}$$

Without tedious and perhaps impossible observation tasks one does not know where the next microcrack will form and therefore ρ_k or δ are not known. It is known, however, that $[(S)/90_n]_s$ laminates tend to form roughly periodic microcracks. We thus might expect $\rho_k \approx \langle\rho\rangle$ and $\delta \approx \langle\rho\rangle/2$. Liu and Nairn [23], however, point out that these approximations are an oversimplification. From Equation 5 it can be calculated that the energy release rate is higher when the microcrack forms in a large microcrack interval than it is when it forms in a small microcrack interval. It is logical to assume the microcrack formation prefers locations that maximize energy release rate. Thus when there is a distribution in crack spacings, the next microcrack will prefer to form in a crack interval that is larger the the average crack spacing. Liu and Nairn [23] introduced a factor f defined as the average ratio of the crack spacing where the microcrack forms to the average crack spacing. By this assumption, $Y(D)$ is approximated by

$$Y(D) \approx \chi(2f\langle\rho\rangle/2) - \chi(f\langle\rho\rangle) \tag{8}$$

The f factor can be treated as an adjustable parameter when fitting microcracking results to Equation 5 Using f values between 1.0 and 1.44, Liu and Nairn [23] find good fits to results from a wide variety of laminates. Fortunately, the value of f selected to get the best fit does not influence the calculated fracture toughness, G_{mc}. In this section, we treat f as a layup independent factor that is approximately 1.2. In a latter section we describe a tedious experimental procedure to measure f.

Solving Equation 5 for a given material

$$\sigma_0 = \frac{1}{k_m^{(1)}}\left(\sqrt{\frac{G_{mc}}{C_3 t_1 Y(D)}} - k_{th}^{(1)}T\right) \tag{9}$$

There are three unknowns in Equation 9: G_{mc} or the microcracking fracture toughness, T or the temperature differential that determines the level of residual thermal stresses, and f in the definition of $Y(D)$. T can be

measured by various means, or when it is not available it can be estimated from knowledge of the processing conditions. For AS4/3501-6 laminates we estimated $T = -125°\text{C}$ [23]. When f is not measured it can be assumed to be approximately 1.2. We are left with one unknown: G_{mc}. If Equation 9 provides a *fundamental* analysis of microcracking, it should be possible to predict the results from all $[(S)/90_n]_s$ laminates using a single value of G_{mc}.

We applied Equation 9 to the eight $[(S)/90_n]_s$ laminates tested in this study. We found that all eight could be fit with $G_{mc} = 280$ J/m^2. This paper focuses on the master curve analysis of this data. The reader is therefore referred to [23] and [30] for typical fits of Equation 9 to raw plots of microcrack density *vs.* applied stress. All eight fits were determined to be good. The only discrepancies appeared at low crack density. These were attributed to laminate flaws that are not explicitly included in the analysis [23, 30]. The newly determined value of G_{mc} agrees well with previously measured results for this material by Liu and Nairn [23] ($G_{mc} = 240$ J/m^2) and by Yalvac *et. al.* [24] ($G_{mc} = 230$ J/m^{2}2).

4.2. $[90_n/(S)]_s$ laminates: Energy release rate analysis

The variational mechanics stress analysis of $[90_n/(S)]_s$ laminates is complicated by the loss of symmetry resulting from staggered microcracks. Nairn and Hu [25] extended Hashin's [40, 41] analysis to the staggered microcracking pattern in Fig. 3B. Their results can be cast in a form similar to the $[(S)/90_n]_s$ laminate results. The tensile stress in the 90° plies on the left of Fig. 3B is

$$\sigma_{xx}^{(1)}(\xi) = \sigma_{x0}^{(1)}\left(1 - \phi_a(\xi)\right) \tag{10}$$

where $\phi_a(\xi)$ is a new function defined by variational analysis (see the Appendix). The subscript "a" denotes antisymmetric damage. Likewise the total strain energy release rate associated with an increase in microcracking damage is

$$G_m = {\sigma_{x0}^{(1)}}^2 C_{3a} t_1 Y_a(D) \tag{11}$$

where C_{3a} is a constant defined in the Appendix and

$$Y_a(D) = LW\frac{d}{dA}\frac{\sum_{i=1}^{N}\chi_a(\rho_i)}{\sum_{i=1}^{N}\rho_i} = \frac{d}{dD}\Big(D\langle\chi_a(\rho)\rangle\Big) \tag{12}$$

In Equation 12, the function $\chi_a(\rho)$, which is determined by variational analysis (see the Appendix), is the antisymmetric damage state analog of $\chi(\rho)$. Accounting for the staggered crack geometry and using the same approximations that were successful for $[(S)/90_n]_s$ laminates, $Y_a(D)$ can be approximated by [25]

$$Y_a(D) \approx \frac{1}{2}\left(3\chi(f\langle\rho\rangle/3) - \chi(f\langle\rho\rangle)\right) \tag{13}$$

Equation 9, with $Y(D)$ replaced by $Y_a(D)$, is the prediction for crack density as a function of applied stress. To test the predictions, we compared the experimental results for the ten laminates with sufficient microcracking data to the theoretical predictions. In fact, we have a more rigorous test for $[90_n/(S)]_s$ laminates than we did for $[(S)/90_n]_s$ laminates because the results on $[(S)/90_n]_s$ laminates can be viewed as experiments that measured $G_{mc} = 280$ J/m^2. If Equation 11 correctly accounts for outer-ply 90° plies and staggered microcracks, then it should be possible to fit experimental results for $[90_n/(S)]_s$ laminates with the same value of G_{mc}. Because results for crack density *vs.* applied stress for $[90_n/(S)]_s$ laminates have only rarely appeared in the literature, we give one plot of the comparison between theory and experiment in Fig. 2. The results in Fig. 2 are for $[90/0_n]_s$ laminates with $n = 0.5$, 1, 2, and 4; they are analyzed with the assumptions that $T = -125°\text{C}$ and $f \approx 1.2$. All results are fit well with a single value of $G_{mc} = 240$ J/m^2. This microcracking fracture toughness is lower than the toughness used to fit the results for $[0_n/90_m]_s$ but close enough to be within experimental uncertainty. It agrees better with the results of Liu and Nairn [23] and Yalvac *et. al.* [24]. In general, fits for $[(S)/90_n]_s$ laminates are slightly better than fits for $[(S)/90_n]_s$ laminates.

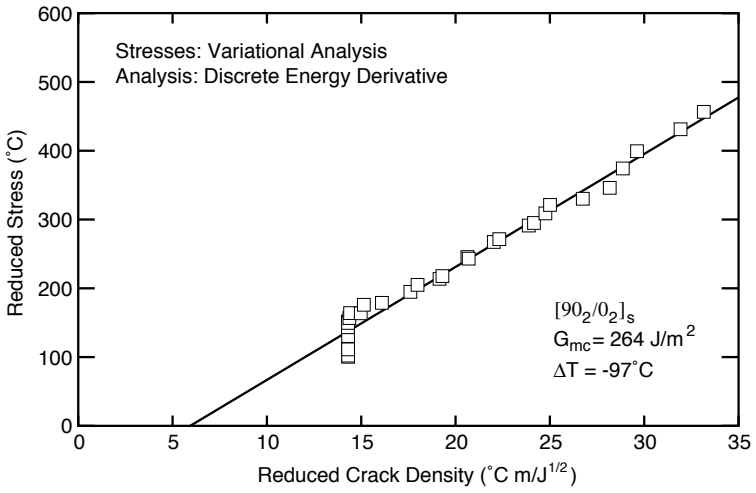

Fig. 4. A master curve analysis of a $[90_2/0_2]_s$ AS4/3501-6 laminate. The energy release rate is calculated with a discrete energy derivative defined by $Y_a(D)$ in Eq. (13) using $f = 1.2$.

4.3. Master curve analysis

Multiplying Equation 9 by $-k_m^{(1)}/k_{th}^{(1)}$ gives

$$-\frac{k_m^{(1)}}{k_{th}^{(1)}}\sigma_0 = -\frac{1}{k_{th}^{(1)}}\sqrt{\frac{G_{mc}}{C_3 t_1 Y(D)}} - T \tag{14}$$

This equation leads us to define a reduced stress density and a reduced crack density as

$$\begin{array}{lrcl} \text{reduced stress:} & \sigma_R & = & -\frac{k_m^{(1)}}{k_{th}^{(1)}}\sigma_0 \\ \text{reduced crack density:} & D_R & = & -\frac{1}{k_{th}^{(1)}}\sqrt{\frac{1}{C_3 t_1 Y(D)}} \end{array} \tag{15}$$

A plot of σ_R *vs.* D_R defines a master plot for microcracking experiments. If the variational analysis and energy release rate failure criterion are correct, a plot of σ_R *vs.* D_R will be linear with slope $(G_{mc})^{1/2}$ and intercept T. Because G_{mc} and T are layup independent material properties, the results from all laminates should fall on the same linear master plot. A critical test of the variational analysis microcracking theory is to determine if the master curve is linear and if all laminates fall on the same line. Furthermore, the resulting slope and intercept must define physically reasonable quantities.

A typical master curve analysis for a single $[90_2/0_2]_s$ laminate is shown in Fig. 4. The master plot is linear except for a few points at the lowest crack density. As previously discussed, the low crack density results are affected by processing flaws that are not included in the microcracking analysis [23]. It is not surprising that they deviate from the master curve, and they should be ignored when measuring G_{mc}. The straight line in Fig. 4 is the best linear fit that ignores the low crack density data. The slope gives $G_{mc} = 264$ J/m^2 which agrees with the fits to raw data in the previous section and with the results in other studies [23, 24]. The slope gives $T = -93^\circ$C, which is reasonable and is similar to the previously assumed value of $T - 125^\circ$C [23]. Note that a side benefit of the master curve analysis is that the value of T does not have to be assumed or measured. It can, in effect, be measured by analysis of the microcracking data. We comment more on measuring T in the Section 5.

Figure 5 gives the master plot for all 18 laminates tested in this study. We assumed that $f = 1.2$ for all laminates and we ignored data with crack densities less than 0.3 mm^{-1}. We claim Fig. 5 verifies both the validity of an energy release rate failure criterion and the accuracy of the variational analysis calculation of G_m in Equations 5 and 11. Three facts support this claim. First, all laminates fall on a single master curve plot within a relatively narrow scatter band. We discuss the scatter more below. Secondly, the results for $[90_n/(S)]_s$ laminate (open symbols) agree with the results for $[90_n/(S)]_s$ laminates (solid symbols). Thus

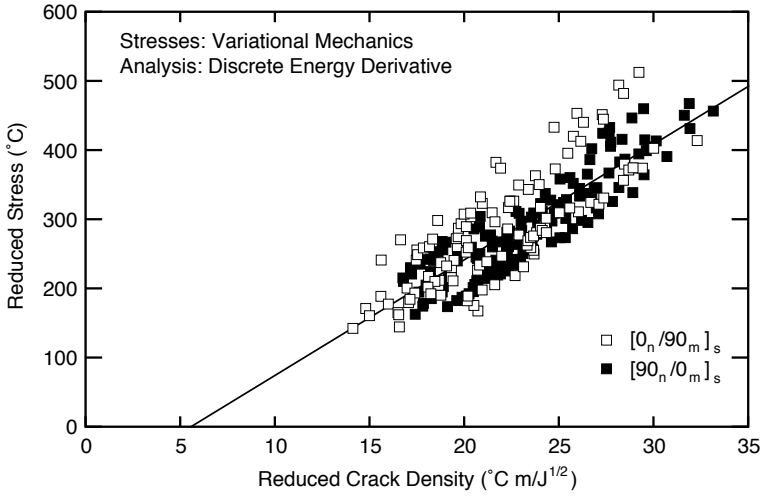

Fig. 5. A master curve analysis of all AS4/3501-6 laminates. The energy release rate is calculated with a discrete energy derivative defined by $Y(D)$ or $Y_a(D)$ in Eqs. (8) and (13) using $f = 1.2$. Data for crack densities less than 0.3 mm^{-1} are not included in this plot.

a single unified analysis can account for both the symmetric damage state in $[(S)/90_n]_s$ laminates and the antisymmetric damage state in $[90_n/(S)]_s$ laminate. Thirdly, the slope and the intercept of the global linear fit in Fig. 5 result in a calculation of $G_{mc} = 279$ J/m^2 and $T = -93$°C. Both of these results are reasonable measured values for these physical quantities.

There is an observable scatter band for the experimental points relative to the global, linear master curve. This scatter band may represent deficiencies in the analysis that need further refinement. Alternatively, we note that the scatter results more from a laminate to laminate variation in intercept than it does from a laminate to laminate variation in slope. It is thus possible that the scatter is due to real variations in T. Physically, $T = T_s - T_0$ and because all laminates were processed under identical conditions, T should be the same for all laminates. T, however, can also be interpreted as the *effective* level of residual thermal stresses. By Equation 3, when $\sigma_0 = 0$ the residual stress in the 90° plies is $\sigma^{(1)}_{xx,th} = k^{(1)}_{th}T$. Although all laminates were processed under identical conditions, the laminates had different thicknesses. If the different thicknesses caused variations in thermal history, it is possible that the level of residual stresses was layup dependent. A layup dependence in T could cause the type scatter observed in Fig. 5.

4.4. Master curve analysis for other microcracking theories

Most previous microcracking theories are based on stress analyses that eliminate the z-dependence of the stress analysis by making various assumptions about the z-direction stress or displacement. The common assumptions are zero stress, zero average stress, or zero displacement. We define any analysis using one of these assumptions as a "one-dimensional" analysis. Examples can be found in Refs. [1, 2, 5, 12, 31–39]. We note that some authors describe their analyses as "two-dimensional" analyses [33, 34, 38, 39]. In all cases, however, the second dimension is the y-dimension whose inclusion is little more than a correction for Poisson's contraction. The difference between a two-dimensional (x–y) plane analysis and a one dimensional x-axis analysis is marginal [30].

The first one-dimensional analysis is described by Garret and Bailey [1]. They used a shear-lag approximation to derive a second order differential equation for total stress transferred from the 90° plies to the (S) sublaminate, $\Delta\sigma$ defined as

$$\Delta\sigma(x) = \left\langle \sigma^{(2)}_{xx}(x) \right\rangle - \sigma^{(2)}_{x0} \tag{16}$$

By using a consistent nomenclature and transposing the equations to the dimensional ξ coordinate, we find that all one-dimensional analysis [1, 2, 5, 12, 31, 32, 35–37] (including the "two-dimensional" (x–y) plane

analyses [33, 34, 38, 39]) can be reduced to a generalized form of Garret and Bailey [1] equation:

$$\frac{d^2\Delta\sigma}{d\xi^2} + \Phi^2\Delta\sigma = \omega(P) \tag{17}$$

where Φ is a constant that depends on laminate properties and material properties and $\omega(P)$ is a function of applied load. The boundary conditions for Equation 17 are

$$\Delta\sigma(\pm\rho) = \frac{t_2\sigma_{x0}^{(1)}}{t_1} \tag{18}$$

The constant Φ governs the rate of stress transfer through shear at the $90/(S)$ interface and we call it the shear-stress transfer coefficient. The function $\omega(P)$ is zero in all analyses except that of Nuismer and Tan [38, 39]. It appears to have little effect on predictions [30]and we set $\omega(P) = 0$ in subsequent calculations.

Equation 17 can easily be solved. The tensile stresses in the 90° plies are identical to Equation 1 except that $\phi(\xi)$ needs to be redefined into a one-dimensional result:

$$\phi_{1D}(\xi) = \frac{\cosh\Phi\xi}{\cosh\Phi\rho} \tag{19}$$

The tensile stresses in the (S) sublaminate and the shear stresses can be found from Equation 19 by force balance and stress equilibrium. The z-direction normal stresses are undefined in one-dimensional analyses. From these stress results, it is possible to propose failure criteria and make predictions about microcracking. In this section we examine the results of several previous one-dimensional microcracking theories.

Garret and Bailey [1] postulated that the next microcrack forms when the maximum stress in the 90° plies, which occurs at $\xi = 0$, reaches the transverse strength of those plies. By this failure criterion, Equations 1 and 19 can be rearranged to give a strength theory master curve

$$-\frac{k_m^{(1)}}{k_{th}^{(1)}}\sigma_0 = -\frac{1}{k_{th}^{(1)}}\frac{\sigma_T}{\big(1-\phi_{1D}(0)\big)} - T \tag{20}$$

where σ_T is the transverse strength of the 90° plies and, as calculated by Garret and Bailey [1], $\Phi = \sqrt{G_{xz}^{(1)}C_1}$. Defining the reduced stress as in Equation 15 and the reduced crack density as

$$\text{reduced crack density :} \qquad D_R = -\frac{1}{k_{th}^{(1)}}\frac{1}{\big(1-\phi_{1D}(0)\big)}, \tag{21}$$

and using a master-curve analysis, Equation 20 predicts that a plot of σ_R *vs.* D_R should be linear with slope σ_T and intercept T.

The result of a strength theory analysis applied to our experimental results is in Fig. 6. The master-curve analysis shows the theory to be very poor. The results from individual laminates are somewhat non-linear and they do not overlap the results from other laminates. Furthermore, the results from $[(S)/90_n]_s$ (open symbols) and $[90_n/(S)]_s$ (filled symbols) laminates segregate into two groups. This segregation is a characteristic of all one-dimensional analyses. Any analysis that ignores the z-dependence of the stress analysis will fail to make a distinction between inner and outer 90° ply groups. We therefore conclude that no model based on a one-dimensional stress analysis can successfully predict results for both $[(S)/90_n]_s$ and $[90_n/(S)]_s$ laminates. If we draw the best line through the data in Fig. 6, the slope and intercept give $\sigma_T = 15.2$ MPa and $T = +192$°C. These results are unreasonable because the transverse tensile strength of AS4/3501-6 laminates is higher than 15.2 MPa and T must be less than zero for laminates cooled after processing.

There are two problems with the Garrett and Bailey model. First, it uses a one- dimensional shear-lag stress analysis. Secondly it uses a poor failure criterion. To investigate the limitation of the stress analysis, we implemented the strength model using the two-dimensional variational analysis. This approach still gave poor results. The poor results with the more accurate stress analysis suggests that it is the use of a strength failure criterion that is the more serious and fundamental problem with this analysis. There have been some

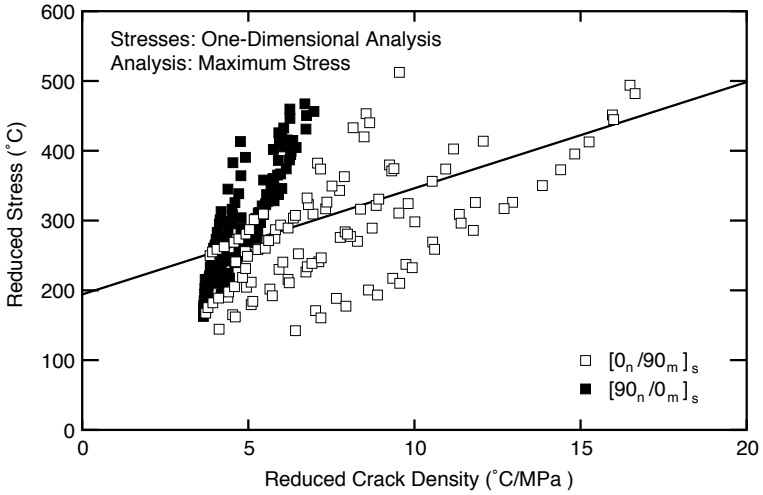

Fig. 6. A master curve analysis of all AS4/3501-6 laminates a maximum stress failure criterion and a one-dimensional stress analysis. Data for crack densities less than 0.3 mm^{-1} are not included in this plot.

attempts to develop more sophisticated strength models, such as probabilistic strength models [9, 13, 22, 34, 43]. These models, however, have been found to require em in situ laminate strength properties and therefore would also give poor master curves [30]/ We suggest that strength models cannot adequately predict failure in composite laminates.

Because of the problems with all strength analyses, numerous authors have suggested energy failure criteria for predicting microcracking[3, 5, 17, 20, 23, 25, 30, 35–37, 39, 42]. Although energy release rate failure criteria were first proposed for microcrack initiation [3, 5, 17], Caslini *et. al.* [20] were the first to suggest using total microcrack energy release rate to predict microcrack density as a function of applied load. They used a one-dimensional analysis that assumes parabolic displacements in the 90° plies [31, 32] to express the structural modulus as a function of crack density. They treated crack area, $A = 2t_1WLD$, as a continuous variable and differentiated the modulus expression to find energy release rate. Because they take an analytical derivative as a function of crack area, we refer to this approach as the *analytical derivative approach*. By treating Equation 5 as a definition of $Y(D)$, the Caslini *et. al.* [20] result for G_m can be expressed using

$$Y_{1D,a}(D) = \frac{C_1}{C_3\Phi}\left(\tanh\Phi\rho - \Phi\rho\,\text{sech}^2\Phi\rho\right) \tag{22}$$

where subscript "$1D, a$" denotes one-dimensional stress analysis and an analytical derivative approach, and $\Phi = \sqrt{3G_{xz}^{(1)}C_1}$. Han *et. al.* [35, 36] describe a similar analysis, but used crack-closure methods to calculate G_m. Because their results are identical to Caslini *et. al.* [20], the Han *et. al.* approach [35, 36] is also an analytical derivative model. Finally, we note that the seemingly more realistic stress analysis that assumes parabolic displacement in the 90° plies [31, 32, 35, 36] unfortunately only result in a trivial change in Φ by a factor of $\sqrt{3}$ when compared to the simple Garrett and Bailey [1] analysis.

By replacing $Y(D)$ with $Y_{1D,a}(D)$ we can evaluate the microcracking models in [20, 35, 36]. The results of such an analysis applied to our experimental results are in Fig. 7. This master curve was the worst of any model we evaluated. The results from individual laminates are fairly linear but there give slopes and intercepts corresponding to toughnesses as high as 10^{12} J/m^2 and values of T that imply specimen temperatures always well below absolute zero. These are clearly unreasonable results. The least-squares linear fit through the data in Fig. 7 gives $G_{mc} = 2$ J/m^2 and $T = 323$°C. The global fit does not pass through the data (because the data from different laminates do not overlap) and the global fitting constants are unrealistic.

In Section 4.3, we argued that Caslini *et. al.*'s [20] original suggestion about analyzing microcracking using energy release rate is appropriate. We are left with explaining why their energy release rate approach is a complete failure. Our first attempt was to use the variational mechanics stress analysis and calculate G_m by

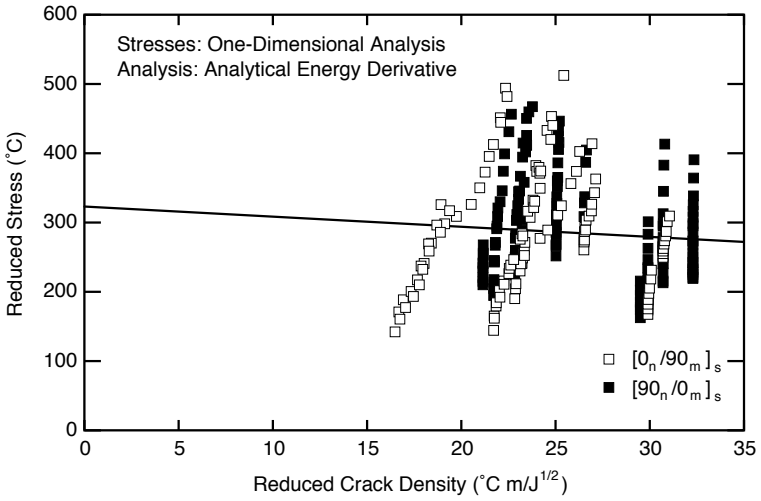

Fig. 7. A master curve analysis of all AS4/3501-6 laminates using an analytical derivative energy release rate failure criterion and a one-dimensional stress analysis. Data for crack densities less than 0.3 mm^{-1} are not included in this plot.

a similar analytical derivative approach. This made slight improvements in the master curve, but the overall quality and the fitting constants were still terrible. We suggest instead that the analytical derivative approach is non-physical and therefore $Y_{1D,a}(D)$ gives the wrong energy release rate. The analytical-derviative, energy release rate at a given crack density corresponds the the unlikely fracture event whereby all cracks close and then reopen again as periodic cracks with a slightly higher crack density. In real microcracking, one microcrack forms between two existing straight microcracks. Apparently the energy release rate for this process is dramatically different than that calculated with an analytical derivative.

Laws and Dvorak [37] were the first to suggest modeling the actual fracture process. They calculated the change in energy associated with the formation of a new microcrack between two existing microcracks. Because they model a discrete process, we call their approach the *discrete derivative approach*. We cast Laws and Dvorak [37] results in the form of the variational analysis be redefining $Y(D)$ to be

$$Y_{1D,d}(D) = \frac{C_1}{C_3\Phi}\left(2\tanh f\Phi\rho/2 - \tanh f\Phi\rho\right) \tag{23}$$

where subscript "$1D, d$" denotes one-dimensional stress analysis and a discrete derivative approach and f is the factor introduced in the variational analysis to account for the tendency of microcracks to prefer larger than average microcrack intervals. Following Reifsnider [2], Laws and Dvorak [37] used a shear-lag that assumes an interlayer of unknown thickness and stiffness between the (S) sublaminate in the 90° plies. Their Φ can be expressed as

$$\Phi = \sqrt{\frac{Gt_1C_1}{t_0}} \tag{24}$$

where G is the shear modulus of the interlayer and t_0 is its thickness.

By replacing $Y(D)$ with $Y_{1D,d}(D)$ we can evaluate the Laws and Dvorak microcracking mode [37]. A drawback of their analysis is that the effective stiffness of the interlayer is an unknown parameter. Laws and Dvorak [37] suggest a circular scheme in which G/t_0 is determined by prior knowledge of G_{mc} and the stress required to form the first microcrack. Because of our concern about the sensitivity of low-crack-density results to laminate processing flaws, we used the high-crack-density results from the single laminate in Fig. 4 to determine G/t_0. We varied G/t_0 until the slope of the Laws-and-Dvorak analysis master curve [37] gave G_{mc} equal to the variational analysis result of 280 J/m^2. This exercise yielded $G/t_0 = 4000$ N/mm, a linear master curve, and an intercept of −73°C. These initial results were promising. The results of master plot analysis applied to our experimental results using $Y_{1D,d}(D)$, $G/t_0 = 4000$ N/mm, and $f \approx 1.2$ are in Fig. 8. This master-curve analysis is the most satisfactory of all the previous literature models but still have serious

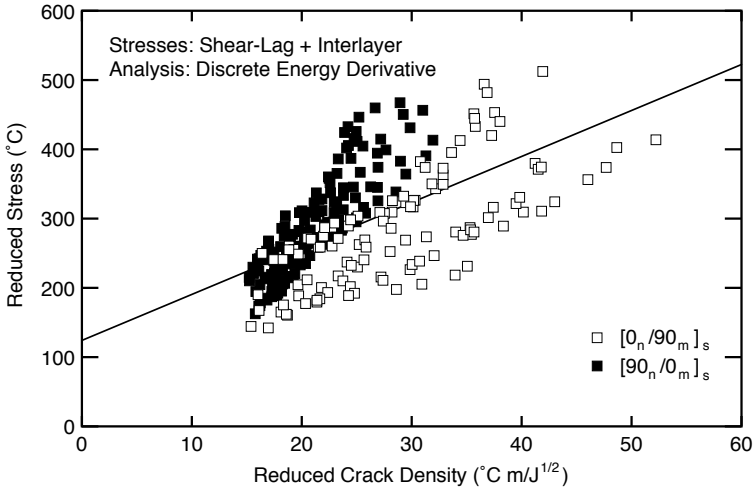

Fig. 8. A master curve analysis of all AS4/3501-6 laminates using a discrete derivative energy release rate failure criterion and a one-dimensional stress analysis. Data for crack densities less than 0.3 mm^{-1} are not included in this plot.

problems. Most importantly, the results from individual lamina do not overlap. As is characteristic of one-dimensional analyses, the results from $[(S)/90_n]_s$ and $[90_n/(S)]_s$ laminates segregate into two groups. The least-squares linear fit through the data in Fig. 8 gives $G_{mc} = 44$ J/m^2 and $T = +124$°C. The global fit does not pass through the data (because the data from different laminates do not overlap) and the global fitting constants are unreasonable.

We believe the only problem with the Laws and Dvorak [37] is its use of an oversimplified, one-dimensional stress analysis. If their failure criterion is implemented with the variational mechanics stress analysis, the result is equivalent to the analysis first presented in Nairn [42]. As shown in Section 4.3, such an analysis gives a good master plot (see Fig. 5).

It is possible to evaluate many other theories using the master plot approach. One could combine any failure criterion (strength, analytical derivative G_m, or discrete derivative G_m) with any stress analysis (one-dimensional analyses, two-dimensional variational analyses, or refined variational analysis [44]). We tried many such combinations and found that all attempts at using one-dimensional stress analyses are complete failures. If nothing else, they always fail to differentiate between $[(S)/90_n]_s$ and $[90_n/(S)]_s$ laminates. When more accurate stress analyses, such as variational analysis, are used, all attempts at using strength or analytical-derivative G_m failure criteria are also complete failures. We finally concluded that only the specific combination of a sufficiently accurate stresses analysis (*e.g.*, variational stress analysis) with a discrete derivative evaluation of G_m is capable of producing a meaningful master plot.

4.5. The effect of distribution of microcrack spacings

One difficulty in analyzing microcracking is the need for the f factor to account for the effect of a distribution in crack spacings. We treated f as an adjustable parameter, but found that it is layup independent and usually $f \approx 1.2$. Fortunately, the precise choice of f has only a second order effect on the measured value of G_{mc}. When we varied f from 1.1 to 1.7, the master plot slope gave G_{mc}'s from 204 J/m^2 to 333 J/m^2 or $G_{mc} = 270 \pm 70$ J/m^2. Thus, the microcracking toughness of any material can be reasonably characterized without being concerned with detailed knowledge f factor. For more precise work, however, measuring f may be warranted. In this section we describe one technique for measuring f. When successful, this technique supports the claim that the f parameter has physical meaning and is not merely an adjustable fitting parameter.

In principle, the need for f could be entirely avoiding by directly measuring $Y(D)$. By Equation 6 or 12 we could plot $D\langle\chi(\rho)\rangle$ or $D\langle\chi_a(\rho)\rangle$ as a function of D and numerically differentiate to measure $Y(D)$ or $Y_a(D)$. We tried this approach and found that the inherent difficulties in numerically differentiating fracture

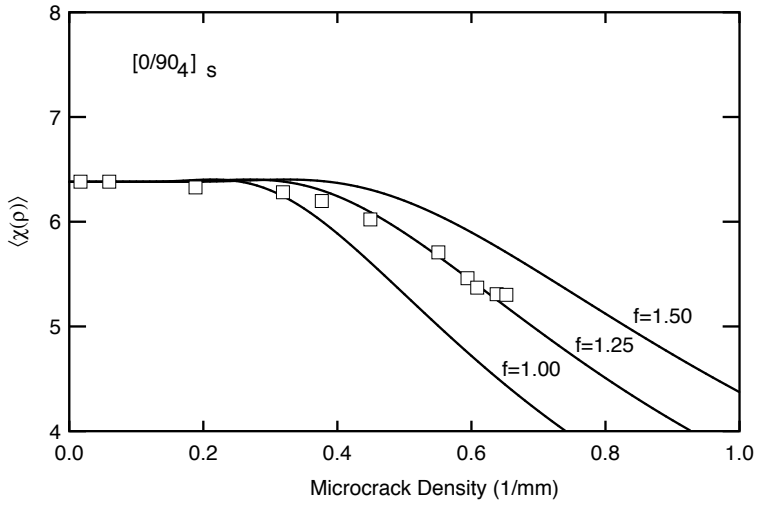

Fig. 9. The measured $\langle\chi(\rho)\rangle$ (symbols) and the predicted $\langle\chi(\rho)\rangle$ (line) for a $[0/90_4]_s$ laminate. The three prediction lines are for $f = 1.00$, $f = 1.25$, and $f = 1.50$. The best prediction to the experimental results was when $f = 1.25$

data made it an impractical approach. To avoid the differentiation step, we developed an integral approach. We treated Equation 8 and 13 as single-parameter representations of $Y(D)$. Inserting $Y(D)$ in Equation 8 into Equation 6 gives

$$\frac{d\,\langle\chi(\rho)\rangle}{dD} = \frac{2\chi(f\rho/2) - \chi(f\rho) - \langle\chi(\rho)\rangle}{D} \tag{25}$$

This first order differential equation can easily be integrated to predict $\langle\chi(\rho)\rangle$ as a function of D for any value of f. By comparing the prediction to experimental results it is possible to measure f. An advantage over the direct measurement of $Y(D)$ is the the experimental determination of $\langle\chi(\rho)\rangle$ does not require any numerical differentiation. A similar treatment can also be applied to $[90_n/(S)]_s$ laminates using $Y_a(D)$ and $\chi_a(\rho)$ along with Equations 13 and 12.

In brief, when each test was periodically stopped to find the crack density, we also did the tedious task of measuring the complete distribution of crack spacings. From $\rho_1, \rho_2, \ldots, \rho_N$ at each crack density, we calculated $\langle\chi(\rho)\rangle$ as a function of D. In a simple computer program, we varied f until the predicted $\langle\chi(\rho)\rangle$ agreed with the measured $\langle\chi(\rho)\rangle$. Some typical results are in Fig. 9. The symbols are experimental points and the three smooth lines are predictions for $f = 1.00$, $f = 1.25$, and $f = 1.50$. At low crack density $\langle\chi(\rho)\rangle$ is constant and the predictions are independent of f. The low crack density data cannot be used to measure f. At higher crack density $\langle\chi(\rho)\rangle$ begins to decrease. The onset and rate of decrease are a sensitive functions of f. For the laminate in Fig. 9, a value of $f = 1.25$ predicted the complete experimental curve. This result suggests that the single-parameter representation of $Y(D)$ is reasonable accurate. If it were not, a single value of f could not predict the results. The curves for $f = 1.00$ and $f = 1.50$ illustrate the precision in measuring f. There is enough sensitivity in the high crack density data to estimate the precision in f for this laminate as $f = 1.25 \pm 0.05$.

We did the measurement shown in Fig. 9 for each laminate in this study and got good results for most $[(S)/90_n]_s$ laminates. The measured f values ranged from 1.15 to 1.35. These f values agreed well with the value of $f \approx 1.2$ that was previously determined by fitting theory with f as an adjustable parameter (see Fig. 2). For some $[(S)/90_n]_s$ laminates the experimental results only included low crack density data. As shown in Fig. 9, the low crack density results are insensitive to f and thus the data from these laminates could not be used to measure f. Our attempts to measure f in $[90_n/(S)]_s$ laminates were less successful. We could predict the onset and rate of the decrease in $\langle\chi(\rho)\rangle$ at high crack density, but the predictions required selecting $f = 1.45$ to 1.9. These f values are inconsistent with fits of theory to raw data that treat f as an adjustable parameter. We do not know the reasons for our inability to measure f in $[90_n/(S)]_s$ laminates. It is possible that our measurement of $\langle\chi(\rho)\rangle$ was oversimplified. By averaging $\chi_a(\rho)$ we were implicitly assuming that there is perfect stagger. In other words, we assumed that all crack intervals appeared as in

Fig. 3B where the crack in one 90° ply groups is exactly centered between two microcracking in the other 90° ply group. A more precise calculation of $\langle\chi(\rho)\rangle$ that accounts for imperfect stagger might result in better f values.

5. Discussion and conclusions

It is relatively easy to fit approximate theories to a single set of experimental results from one or two laminates. When theories are required to simultaneously fit results from 18 different laminates, however, the task is much harder. Our large data base thus allowed us to make a critical evaluation of various microcracking theories. We found that of existing theories, only an energy-based failure criterion implemented using a discrete evaluation of the energy release rate and a two-dimensional variational stress analysis was capable of analyzing all results. The differences between various theories were best visualized using a master plot analysis. Those master curves showed that the differences between the theories are not subtle. All attempts at using one-dimensional stress analyses, regardless of the failure criterions, were very poor. Even the more accurate variational analysis gave poor results when it was used to predict failure with an inappropriate failure criterion. The variational analysis and discrete energy release rate method we recommended can viewed as not only the best model but also as the only acceptable model. Of course, additional models that build on the recommended approach while refining variational analysis [44] would also produce acceptable results.

A crucial aspect of any microcracking theory is the failure criterion used to generate the predictions. We tried many failure criteria and found that only a fracture mechanics failure criterion based on the actual fracture process provided a fundamental interpretation of all results. The fracture mechanics criterion is that microcracking occurs when the energy release rate associated with the formation of the next microcrack exceeds the microcracking toughness of the material. It is important that the calculated energy release rate corresponds to the actual fracture process. For microcracking this involves modeling the fracture event of a new microcracking forming between two existing microcracks. One approach that ignores the actual fracture process is to treat crack density as a continuous variable and analytically differentiate strain energy to get a *pseudo*-energy release rate. The analytical derivative approach ignores the actual fracture process and does not agree with experimental results.

Maximum stress or maximum strain failure criteria were particular bad. Our results substantiate this conclusion for microcracking experiments, but the conclusion is probably more general. We suggest that simple maximum stress or even more sophisticated quadratic failure criteria are not based on energy principles of fracture mechanics, and have no fundamental physical basis, and therefore should not be expected to give useful predictions about composite failure. For example, many laminates plate analyses predict the onset of failure using first-ply failure criteria that are based on simple maximum stress rules. The initiation of microcracking in this paper can be viewed as an experimental study into first-ply failure. The inability of strength models to make any useful predictions about our experimental results is verification that first-ply failure models are inappropriate. If first-ply failure models are inappropriate, we further suggest that more complicated composite failure theories that are rooted in simple strength rules are equally inappropriate.

We found that a good failure criterion alone is not sufficient to develop a successful analysis of microcracking. The failure criterion must be used in conjunction with some stress analysis before it can give predictions. That stress analysis must be sufficiently accurate to insure good results. We found, for example, that the qualitative stresses calculated by one-dimensional stress analysis always gave poor results. The results were poor even when coupled with the best failure criterion as in the model of Laws and Dvorak [37]. In contrast, the more accurate two-dimensional, variational stress analysis coupled with the best failure criterion gave good results. If one plots the stresses calculated by a one-dimensional analysis and those calculated by a variational analysis, the differences are marked, but hardly dramatic [30]. We were thus initially surprised by the dramatic differences between predictions based on the two analyses. A qualitative interpretation of the differences can follow from realizing that fracture is an instability event. When calculating instability processes, minor differences in input stresses can lead to dramatic differences in predictions. In other words, the increased accuracy in stresses attributed to the variational analysis was crucial to the predictions of microcracking.

The master curve analysis in Fig. 5 provides a new technique for measuring a useful material property — the microcracking or *intralaminar* toughness of a composite material. Although it is truly a measured

property, the numerical accuracy of G_{mc} depends on the accuracy of G_m in Equations 5 and 11. To verify the measured G_{mc} using independent experiments we measured the *transverse* fracture toughness of unidirectional AS4/3501-6 laminates. By *transverse* toughness we mean the material toughness for a crack running parallel to the fibers, but normal to the plies. In other words, the propagation of an *intralaminar* crack. The *transverse* toughness was measured using a conventional double-cantilever beam used for delamination specimens and rotating it by 90° so that the previous *interlaminar* crack becomes an *intralaminar* crack. The results were analyzed using the DCB specimen analysis recommended by Williams *et. al.* [45]. The resulting transverse toughness was $G_{tc} = 309$ J/m^2, which is close to $G_{mc} = 279$ J/m^2 determined in Fig. 5. It is noteworthy that both G_{mc} and G_{tc} are significantly higher than the delamination fracture toughness which is $G_{Ic} = 175$ J/m^2 [46]. Experience with other material systems shows that G_{mc} is usually similar to G_{Ic}. Closer inspection, however, reveals that G_{Ic} can be significantly less or significantly greater the G_{mc} depending on structural and material variables [30].

There are three practical details worthy of discussion. First the intercept of the master plot in Equation 14 is T which defines the *effective* level of residual stress in the specimen. In principle, a master curve analysis of microcracking experiments provides a measure of both G_{mc} and of the level of residual stress in the specimen. The results in Figs. 4 and 5 show that residual stresses can be reliably measured. When the results from individual laminates are considered alone, however, the resulting measurement of T is sensitive to small experimental scatter. For the 18 laminates in this study, individual master curves gave T ranging from -33°C to -297°C. The master curve analysis can thus not be recommended as an accurate way to measure residual stresses. For most accurate work, we recommend measuring T and plotting a modified reduced stress of

$$\text{reduced stress}: \qquad \sigma_R = -\frac{k_m^{(1)}}{k_{th}^{(1)}} - T \tag{26}$$

vs. reduced crack density. The resulting plot should be linear and pass through the origin with slope $(G_{mc})^{1/2}$. Fits of such master curves that are forced to pass through the origin can give greater precision in G_{mc} and smaller laminate-to-laminate variability in measured G_{mc}. This approach has the side-benefit of producing master curves for laminate with real variations in T that would otherwise not fall on a single master curve.

Following the suggestion of Liu and Nairn [23], we assumed that low crack density data was dominated by specimen flaws and should be eliminated from the master curve analysis when measuring the material toughness. The second point to discuss is whether the decisions regarding which points to eliminate influenced the results. The low crack density points are relatively few in number and are all clustered around the same reduced crack density (see Fig. 4). Fortunately the global fit to all experimental points is nearly unaffected by inclusion or elimination of the low crack density results. For the most accurate results we recommend eliminating them. It is easy to decide which points should be eliminated by determining which low crack density points deviate from the predicted master curve line.

The third point is the undetermined f factor. Our experiments on $\langle\chi(\rho)\rangle$ show that f is not a fudge factor to produce better fits, but rather a meaningful physical constant. The use of an f factor is an approximate method that accounts for the effect of variations in microcrack spacings which occur in all real laminates. Without the f factor, the analysis would be insensitive to variations in microcrack spacings, and would thus be incapable of predicting their effect on fracture properties. The f factor, therefore, should not be viewed as a limitation of the variational analysis model, but rather as a manifestation of its ability to include crack spacing variation effects. Furthermore, one should question the validity of any microcracking analysis that does not include a similar factor or does not include some method for dealing with variations in crack spacings.

Acknowledgments

This word was supported in part by a contract from NASA Langley Research Center (NAS1-18833) monitored by Dr. John Crews, in part by a gift from ICI Advanced Composites monitored by Dr. J. A. Barnes, and in part by a gift from the Fibers Department of E. I. duPont deNemours and Company monitored by Dr. Alan R. Wedgewood.

References

1. K. W. GARRETT AND J. E. BAILEY, *J. Mat. Sci* **12** (1977) 157.
2. K. L. REIFSNIDER, *Proc. 14th Annual Meeting of SES, Lehigh, PA, November* (1977) 373.
3. A. PARVIZI, K. W. GARRETT, AND J. E. BAILEY, *J. Mat. Sci.* **13** (1978) 195.
4. A. PARVIZI AND J. E. BAILEY, *J. Mat. Sci.* **13** (1978) 2131.
5. J. E. BAILEY, P. T. CURTIS AND A. PARVIZI, *Proc. R. Soc. Lond. A* **366** (1979) 599.
6. M. G. BADER, J. E. BAILEY, P. T. CURTIS, AND A. PARVIZI, *Proc. 3rd Int'l Conf. on Mechanical Behavior of Materials* **3** (1979) 227.
7. F. W. CROSSMAN, W. J. WARREN, A. S. D. WANG, AND G. E. LAW, JR., *J. Comp. Mat Supplement* **14** (1980) 89.
8. W. W. STINCHCOMB, K. L. REFISNIDER, P. YEUNG, AND J. MASTERS, *ASTM STP* **723** (1981) 64.
9. D. L. FLAGGS AND M. H. KURAL, *J. Comp. Mat.* **16** (1982) 103.
10. F. W. CROSSMAN AND A. S. D. WANG, *ASTM STP* **775** (1982) 118.
11. A. L. HIGHSMITH AND K. L. REIFSNIDER, *ASTM STP* **775** (1982) 103.
12. P. W. MANDERS, T. W. CHOU, F. R. JONES, AND J. W. ROCK, *J. Mat. Sci.* **19** (1983) 2876.
13. P.W.M. PETERS, *J. Comp. Mat.* **18** (1984) 545.
14. R. JAMISON, K. SCHULTE, K. L REIFSNIDER, AND W. W. STINCHCOMB, *ASTM STP* **836** (1984) 21.
15. A. S. D. WANG, P. C. CHOU AND S. C. LEI, *J. Comp. Mat.* **18** (1984) 239.
16. A. S. D. WANG, *Comp. Tech. Rev.* **6** (1984) 45.
17. A. S. D. WANG, N. N. KISHORE AND C. A. LI, *Comp. Sci. & Tech.* **24** (1985) 1.
18. M. G. BADER AND LYNN BONIFACE, *Proc.* 5_{th} *Int'l Conf. on Comp. Mat.* (1985) 221.
19. L. BONIFACE, P. A. SMITH, S. L. OGIN, AND M. G. BADER, *Proc* 6^{th} *Int'l Conf. on Comp. Mat.* **3** (1987) 156.
20. M. CASLINI, C. ZANOTTI, AND T. K. O'BRIEN, *J. Comp. Tech & Research* **Winter** (1987) 121. (Also appeared as NASA TM89007, 1986).
21. S. E. GROVES, C. E. HARRIS, A. L. HIGHSMITH, AND R. G. NORVELL, *Experimental Mechanics* **March** (1987) 73.
22. K. C. JEN AND C. T. SUN, *Proc. of the Amer. Soc. Comp,* 5^{th} *Tech. Conf.* (1990) 350.
23. S. LIU AND J. A. NAIRN, *J. Reinf. Plast. & Comp.* **11** (1992) 158.
24. S. YALVAC, L. D. YATS, AND D. G. WETTERS, *J. Comp. Mat.* **25** (1991) 1653.
25. J. A. NAIRN AND S. HU, *Eng. Fract. Mech.* **41** (1992) 203.
26. D. S. ADAMS AND C. T. HERAKOVICH, *J. Thermal Stresses* **7** (1984) 91.
27. D. E. BOWLES, *J. Comp. Mat.* **17** (1984) 173.
28. J. A. NAIRN AND S. HU, *Int. J. Fract.* **57** (1992) 1.
29. S. HU, J. S. BARK, AND J. A. NAIRN, *Comp. Sci. & Tech.* **47** (1993) 321.
30. J. A. NAIRN AND S. HU, in "Damage mechanics of composite materials," edited by R. Talreja (Elsevier Science Publishers, Barking, UK, 1994), p. 187
31. S. L. OGIN, P. A. SMITH, AND P. W. R. BEAUMONT, *Comp. Sci. & Tech.* **22** (1985) 23.
32. S. L. OGIN, P. A. SMITH, AND P. W. R. BEAUMONT, *Comp. Sci. & Tech* **24** (1985) 47.
33. D. L. FLAGGS, *J. Comp. Mat.* **19** (1985) 29.
34. H. FUKUNAGA, T. W. CHOU, P. W. M. PETERS, AND K. SCHULTE, *J. Comp. Mat.* **18** (1984) 339.
35. Y. M. HAN, H. T. HAHN, AND R. B. CROMAN, *Proc. Amer. Soc. of Comp.,* 2^{nd} *Tech. Conf.* (1987) 503.
36. Y. M. HAN, H. T. HAHN, AND R. B. CROMAN, *Comp. Sci. & Tech.* **31** (1987) 165.
37. N. LAWS AND G. J. DVORAK, *J. Comp. Mat.* **22** (1988) 900.
38. R. J. NUISMER AND S. C. TAN, *J. Comp. Mat.* **22** (1988) 306.
39. S. C. TAN AND R. J. NUISMER, *J. Comp. Mat.* **23** (1989) 1029.
40. Z. HASHIN, *Mech. of Mat.* **4** (1985) 121.
41. Z. HASHIN, *Eng. Fract. Mech.* **25** (1986) 771.
42. J. A. NAIRN, *J. Comp. Mat.* **23** (1989) 1106. (See *errata*: *J. Comp. Mat.*, **24**, 233 (1990)).
43. H. FUKUNAGA, T. W. CHOU, K. SCHULTE, AND P. W. M. PETERS, *J. Mat. Sci.* **19** (1984) 3546.
44. J. VARNA AND L. BERGLUND, *J. Comp. Tech. & Res.* **13** (1991) 97.
45. S. HASHEMI, A. J. KINLOCH, AND J. G. WILLIAMS, *Proc. R. Soc. Lond.* **A347** (1990) 173.
46. D. L. HUNSTON, *Comp. Tech. Rev.* **6** (1984) 176.

A Appendix

In the variational mechanics analysis of $[(S)/90_n]_s$ laminates [40, 41, 23, 42] we define the following constants:

$$C_1 = \frac{1}{E_x^{(1)}} + \frac{1}{\lambda E_x^{(2)}} \tag{27}$$

$$C_2 = \frac{\nu_{xz}^{(1)}}{E_x^{(1)}}\left(\lambda + \frac{2}{3}\right) - \frac{\lambda \nu_{xz}^{(2)}}{3E_x^{(2)}} \tag{28}$$

$$C_3 = \frac{1}{60E_z^{(1)}}\left(15\lambda^2 + 20\lambda + 8\right) + \frac{\lambda^3}{20E_z^{(2)}} \tag{29}$$

$$C_4 = \frac{1}{3G_{xz}^{(1)}} + \frac{\lambda}{3G_{xz}^{(2)}} \tag{30}$$

where $E_x^{(i)}$ and $E_z^{(i)}$ are the x- and z-direction moduli of ply group i, $G_{xz}^{(i)}$ is the (x-z) plane shear moduli of ply group i, and $\lambda = t_1/t_2$. Superscripts "(1)" and "(2)" denote properties of the 90° plies and the (S) sublaminate, respectively. t_1 and t_2 are the ply thicknesses defined in Fig. 3. Defining $p = (C_2 - C_4)/C_3$ and $q = C_1/C_3$ there are two forms for the function $\phi(\xi)$ in Equation 1. When $4q/p^2 > 1$

$$\begin{aligned}\phi(\xi) = {} & \frac{2(\beta \sinh\alpha\rho\cos\beta\rho + \alpha\cosh\alpha\rho\sin\beta\rho)}{\beta\sinh 2\alpha\rho + \alpha\sin 2\beta\rho}\cosh\alpha\xi\cos\beta\xi \\ & + \frac{2(\beta\cosh\alpha\rho\sin\beta\rho - \alpha\sinh\alpha\rho\cos\beta\rho)}{\beta\sinh 2\alpha\rho + \alpha\sin 2\beta\rho}\sinh\alpha\xi\sin\beta\xi\end{aligned} \tag{31}$$

where

$$\alpha = \frac{1}{2}\sqrt{2\sqrt{q} - p} \qquad \text{and} \qquad \beta = \frac{1}{2}\sqrt{2\sqrt{q} + p} \tag{32}$$

When $4q/p^2 < 1$

$$\phi(\xi) = \frac{\tanh\alpha\rho\tanh\beta\rho}{\beta\tanh\beta\rho - \alpha\tanh\alpha\rho}\left[\frac{\beta\cosh\alpha\xi}{\sinh\alpha\rho} - \frac{\alpha\cosh\beta\xi}{\sinh\beta\rho}\right] \tag{33}$$

where

$$\alpha = \sqrt{-\frac{p}{2} + \sqrt{\frac{p^2}{4} - q}} \qquad \text{and} \qquad \beta = \sqrt{-\frac{p}{2} - \sqrt{\frac{p^2}{4} - q}} \tag{34}$$

The function $\chi(\rho)$ used in defining the energy release rate for microcracking in $[(S)/90_n]_s$ also has two forms. When $4q/p^2 > 1$

$$\chi(\rho) = 2\alpha\beta(\alpha^2 + \beta^2)\frac{\cosh 2\alpha\rho - \cos 2\beta\rho}{\beta\sinh 2\alpha\rho + \alpha\sin 2\beta\rho} \tag{35}$$

When $4q/p^2 < 1$

$$\chi(\rho) = \alpha\beta(\beta^2 - \alpha^2)\frac{\tanh\alpha\rho\tanh\beta\rho}{\beta\tanh\beta\rho - \alpha\tanh\alpha\rho} \tag{36}$$

In the variational mechanics analysis of $[90_n/(S)]_s$ laminates [25] we define some new constants:

$$C_{2a} = -\frac{\nu_{xz}^{(1)}}{3E_x^{(1)}} + \frac{\nu_{xz}^{(2)}}{E_x^{(2)}}\left(1 + \frac{2\lambda}{3}\right) \tag{37}$$

$$C_{3a} = \frac{1}{20E_z^{(1)}} + \frac{\lambda}{60E_z^{(2)}}\left(8\lambda^2 + 20\lambda + 15\right) \tag{38}$$

$$C_1^* = \frac{1}{E_x^{(1)}} + \frac{(1+2\lambda)^2}{\lambda^3 E_x^{(2)}} \tag{39}$$

$$C_2^* = -\frac{\nu_{xz}^{(1)}}{3E_x^{(1)}} + \frac{\nu_{xz}^{(2)}}{E_x^{(2)}}\left[\frac{(1+2\lambda)(2+\lambda)}{3\lambda}\right] \tag{40}$$

$$C_3^* = \frac{1}{20E_z^{(1)}} + \frac{\lambda}{60E_z^{(2)}}\left(2\lambda^2 + 7\lambda + 8\right) \tag{41}$$

$$C_4^* = \frac{1}{3G_{xz}^{(1)}} + \frac{1 + \lambda + \lambda^2}{3\lambda G_{xz}^{(2)}} \tag{42}$$

The function $\phi_a(\xi)$ that defines the stresses in the 90° plies is expressed in terms of two new functions

$$\phi_a(\xi) = \begin{cases} X_0(\xi) + Y_0(\xi) & \text{if } |\xi| < \rho/2 \\ X_0(\xi) - Y_0(\xi) & \text{if } \rho/2 < |\xi| < \rho \end{cases} \tag{43}$$

Redefining $p = (C_{2a} - C_4)/C_{3a}$ and $q = C_1/C_{3a}$ there are two forms for the function X_0. When $4q/p^2 > 1$

$$\begin{aligned} X_0(\xi) &= \frac{C_3^*\chi^*\left(\frac{\rho}{2}\right)}{C_{3\chi}\left(\frac{\rho}{2}\right) + C_3^*\chi^*\left(\frac{\rho}{2}\right)}\Big[\cosh\alpha\xi\cos\beta\xi - \frac{\alpha\sinh\alpha\rho - \beta\sin\beta\rho}{\beta\sinh\alpha\rho + \alpha\sin\beta\rho}\sinh\alpha\xi\sin\beta\xi \\ &\quad + \frac{\cosh\alpha\rho - \cos\beta\rho}{\beta\sinh\alpha\rho + \alpha\sin\beta\rho}(\alpha\cosh\alpha\xi\sin\beta\xi - \beta\sinh\alpha\xi\cos\beta\xi)\Big] \end{aligned} \tag{44}$$

When $4q/p^2 < 1$

$$\begin{aligned} X_0(\xi) &= \frac{C_3^*\chi^*\left(\frac{\rho}{2}\right)}{C_{3\chi}\left(\frac{\rho}{2}\right) + C_3^*\chi^*\left(\frac{\rho}{2}\right)}\frac{1}{\beta\tanh\frac{\beta\rho}{2} - \alpha\tanh\frac{\alpha\rho}{2}}\Big[\beta\tanh\frac{\beta\rho}{2}\cosh\alpha\xi - \alpha\tanh\frac{\alpha\rho}{2}\cosh\beta\xi \\ &\quad + \tanh\frac{\alpha\rho}{2}\tanh\frac{\beta\rho}{2}(\alpha\sinh\beta\xi - \beta\sinh\alpha\xi)\Big] \end{aligned} \tag{45}$$

In Equations 44 and 45, α, β, and $\chi(\rho)$ are the same as in Equations 32–36 except that the redefined forms of p and q are used. The function $\chi^*(\rho)$ is defined below. For the function $Y_0(\xi)$ we define $p^* = (C_2^* - C_4^*)/C_3^*$ and $q^* = C_1^*/C_3^*$. When $4q^*/{p^*}^2 > 1$

$$\begin{aligned} Y_0(\xi) &= -\frac{C_{3\chi}\left(\frac{\rho}{2}\right)}{C_{3\chi}\left(\frac{\rho}{2}\right) + C_3^*\chi^*\left(\frac{\rho}{2}\right)}\Big[\cosh\alpha^*\xi\cos\beta^*\xi - \frac{\alpha^*\sinh\alpha^*\rho + \beta^*\sin\beta^*\rho}{\beta^*\sinh\alpha^*\rho - \alpha^*\sin\beta^*\rho}\sinh\alpha^*\xi\sin\beta^*\xi \\ &\quad + \frac{\cosh\alpha^*\rho + \cos\beta^*\rho}{\beta^*\sinh\alpha^*\rho - \alpha^*\sin\beta^*\rho}(\alpha^*\cosh\alpha^*\xi\sin\beta^*\xi - \beta^*\sinh\alpha^*\xi\cos\beta^*\xi)\Big] \end{aligned} \tag{46}$$

where α^* and β^* are given by Equation 32 or 34 with p and q replaced by p^* and q^*. When $4q^*/{p^*}^2 < 1$

$$\begin{aligned} Y_0(\xi) &= -\frac{C_{3\chi}\left(\frac{\rho}{2}\right)}{C_{3\chi}\left(\frac{\rho}{2}\right) + C_3^*\chi^*\left(\frac{\rho}{2}\right)}\frac{1}{\beta^*\tanh\frac{\alpha^*\rho}{2} - \alpha^*\tanh\frac{\beta^*\rho}{2}}\Big[\beta^*\tanh\frac{\alpha^*\rho}{2}\cosh\alpha^*\xi \\ &\quad - \alpha^*\tanh\frac{\beta\rho}{2}\cosh\beta^*\xi + \alpha^*\sinh\beta^*\xi - \beta^*\sinh\alpha^*\xi\Big] \end{aligned} \tag{47}$$

The new function $\chi^*(\rho)$ used in the definitions of $X_0(\xi)$ and $Y_0(\xi)$ also has two forms. When $4q^*/{p^*}^2 > 1$

$$\chi^*(\rho) = 2\alpha^*\beta^*\left({\alpha^*}^2 + {\beta^*}^2\right)\frac{\cosh 2\alpha^*\rho + \cos 2\beta^*\rho}{\beta^*\sinh 2\alpha^*\rho - \alpha^*\sin 2\beta^*\rho} \tag{48}$$

When $4q^*/{p^*}^2 < 1$

$$\chi^*(\rho) = \alpha^*\beta^*\left({\beta^*}^2 - {\alpha^*}^2\right)\frac{1}{\beta^*\tanh\alpha^*\rho - \alpha^*\tanh\beta^*\rho} \tag{49}$$

Finally, the function $\chi_a(\rho)$ used in defining the energy release rate for microcracking in $[90_n/(S)]_s$ is defined in terms of $\chi(\rho)$ and $\chi^*(\rho)$ as

$$\chi_a(\rho) = \frac{2\chi\left(\frac{\rho}{2}\right)}{1 + \frac{C_{3\chi}\left(\frac{\rho}{2}\right)}{C_3^*\chi^*\left(\frac{\rho}{2}\right)}} \tag{50}$$